*Micromachining and Microfabrication Symposium, Sept., 21-22, 1998, Santa Clara, CA, Proceedings of SPIE, **Vol. 3512**, pp.215-226*

Linkage Design Effect on the Reliability of Surface Micromachined Microengines Driving a Load

Danelle M. Tanner, Kenneth A. Peterson, Lloyd W. Irwin, Paiboon Tangyunyong, William M. Miller, William P. Eaton, Norman F. Smith, and M. Steven Rodgers

Sandia National Laboratories, P. O. Box 5800, MS 1081, Albuquerque, NM 87185-1081

ABSTRACT

The reliability of microengines is a function of the design of the mechanical linkage used to connect the electrostatic actuator to the drive. We have completed a series of reliability stress tests on surface micromachined microengines driving an inertial load. In these experiments, we used microengines that had pin mechanisms with guides connecting the drive arms to the electrostatic actuators. Comparing this data to previous results[1] using flexure linkages revealed that the pin linkage design was less reliable. The devices were stressed to failure at eight frequencies, both above and below the measured resonance frequency of the microengine. Significant amounts of wear debris were observed both around the hub and pin joint of the drive gear. Additionally, wear tracks were observed in the area where the moving shuttle rubbed against the guides of the pin linkage. At each frequency, we analyzed the statistical data yielding a lifetime (t_{50}) for median cycles to failure and σ, the shape parameter of the distribution. A model was developed to describe the failure data based on fundamental wear mechanisms and forces exhibited in mechanical resonant systems. The comparison to the model will be discussed.

Keywords: micro-mechanical component reliability, micromachine reliability, failure in micromachines, MEMS reliability

1. INTRODUCTION

As MicroElectricalMechanical Systems (MEMS) become deployed in more commercial applications, understanding the reliability issues will be paramount for success. MEMS are typically classified into two types, sensors and actuators. There has been some reliability testing reported for sensors,[2,3] and specifically those that are exposed to harsh environments[4]. There has been some reliability work published on micromachined relays[5]. Recently, a complete review of Texas Instruments' Digital Micromirror Device was published[6]. Data on the lifetime of the Sandia designed microengine has also been reported[7]. The reliability of these MEMS devices is directly tied to the reliability of the microactuator.

The objective of this work was to determine the effect of mechanical linkage design on the lifetime of the microengine driving a load (Figure 1). We have stressed a statistically significant number of microengines driving loads with two different linkages in the Y shuttle. One linkage was a flexure

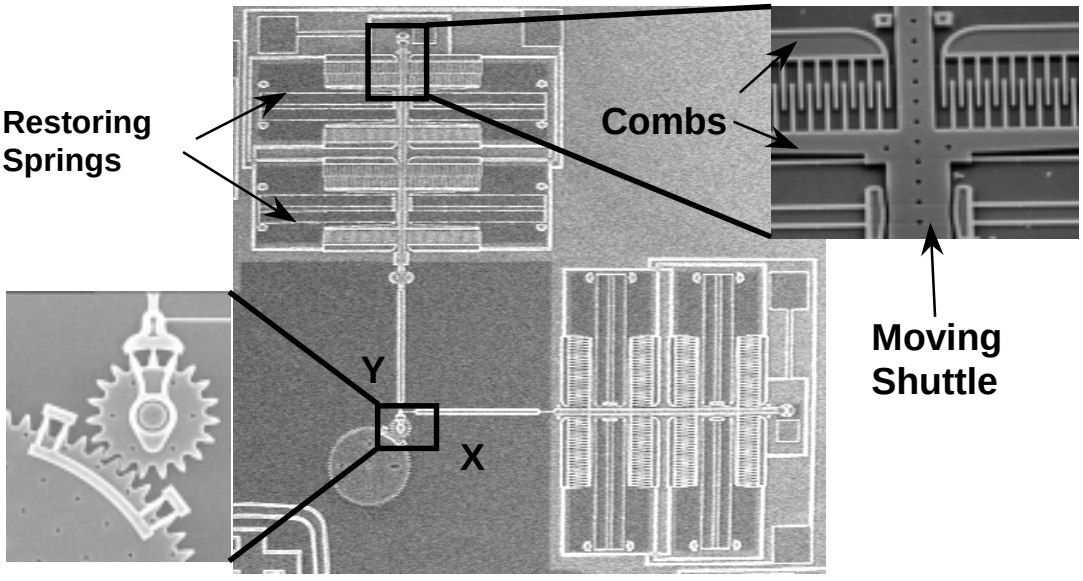

Figure 1. The microengine driving a load with expanded views of the comb drive (top right) and the drive gear and load gear (bottom left) shown in what we define as $\theta = 0$.

with simple guides and the other was a pin mechanism with complex guides.

The comb drives of these microengines have springs that restore any deflections back to the rest position. The polysilicon comb drive exhibits a resonant frequency (the frequency of maximum displacement) like any mechanical oscillating system. By selecting frequencies above and below resonance, we have collected data for the median lifetime of the microengine driving a load as a function of f/f_o where f is the stress frequency and f_o is the resonance frequency.

We compared the lifetime results of the pin linkage design to the predictive models[1] for the number of revolutions to failure for three cases. In this report, we developed two models that are based on the fundamental principles of the physics of wear in a mechanically resonating system. One model describes the adhesive wear at the guides of the pin linkage in the Y shuttle and the other describes the abrasive wear at the same location (described in Section 4.3). We also compared the lifetime results to the drive-gear pin-joint adhesive model developed in Reference 1.

2. MECHANICAL DESIGN

This study used the electrostatically driven microactuator (microengine) developed at Sandia National Laboratories[8]. The microengine consists of orthogonal linear comb drive actuators mechanically connected to a rotating gear as seen in Figure 1. By applying the proper drive voltages, the linear displacement of the comb drives was transformed into circular motion at the drive pin. The X and Y linkage arms are connected to the gear via a pin joint. The gear rotates about a hub that was anchored to the substrate. The microengine has been the focus of much investigation for MEMS devices experiencing sliding friction [1,9].

We used the microengine to drive the load gear depicted in the close-up view as shown in Figure 2. The radius of the microengine drive gear was 38 μm and the load gear was four times as large.

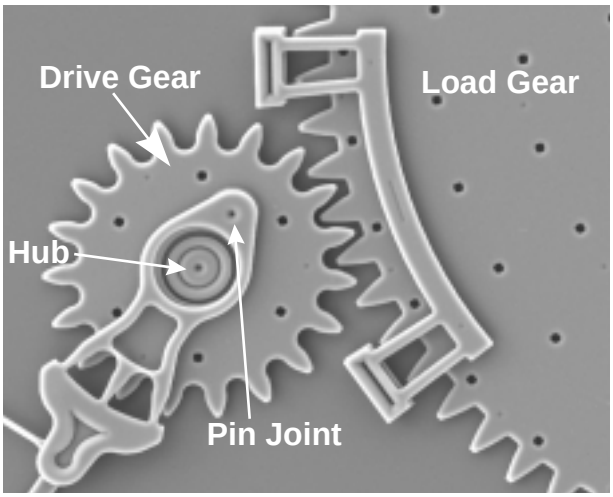

Figure 2. Close-up view of the drive gear meshing with the load gear. The right bracket ( ]) shaped guide on the load gear mitigates out-of-plane wobble to ensure proper meshing of teeth. The hub is anchored to the substrate and the pin joint connects the actuator linkage to the drive gear.

The pin and flexure linkages with guides are shown in Figure 3. The pin is 8 μm in diameter and was located in a 10 μm opening. It is free to move in the vertical direction unlike the pin joint in the drive gear that is constrained. In order to prevent pin displacement in the vertical direction, which would disconnect the shuttle from the linkage arm, the long guides (Figure 10a, right) were added to the design. The long guide is further constrained vertically to 0.5 μm by the use of dimples. The half-round guides constrain the vertical motion of the linkage arm to 2 μm and the lateral motion to 0.5 μm.

The simple guides shown in Figure 3b have only 0.5 μm lateral clearance and no vertical restraint. These guides are typically used for flexure linkage systems where there is no concern about vertical deflection. In this system, the shuttle is connected to the linkage arm by a 2 μm wide, 40 μm long link of polysilicon.

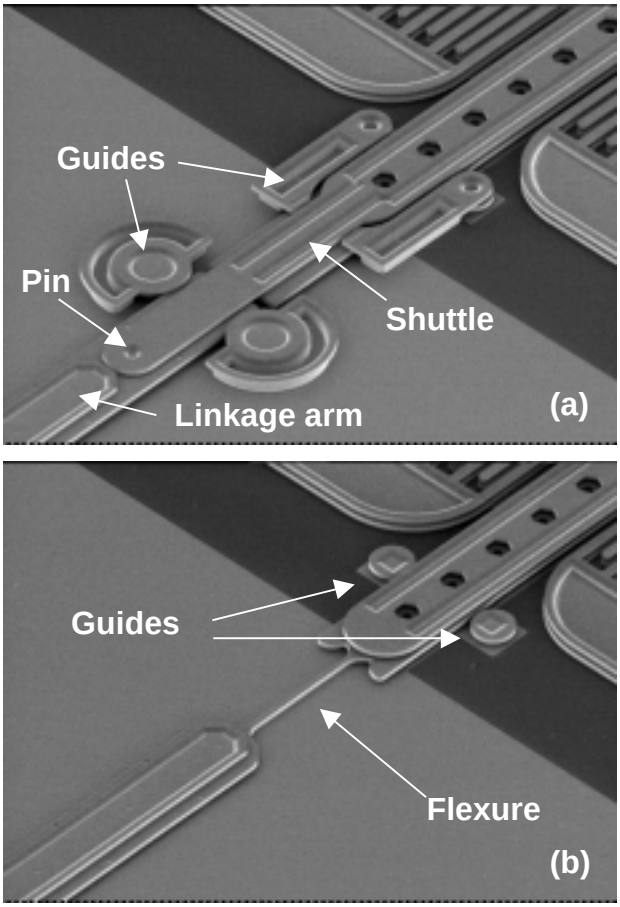

Figure 3. The top SEM shows the pin linkage (a) with guides deemed necessary to control the lateral motion of the shuttle. The lower SEM (b) shows the simpler design of the guides for the flexure linkage type.

3. EXPERIMENT

One of the many issues associated with the reliability of microengines is drive signal parameters.[10] If the drive signals fed to the comb drives are not optimized, there will be excessive forces on the hub and pin joint of the gear, which will lead to early failures.

We characterized the drive parameters fully by measuring both the resonant frequency and the normalized spring constant[9] of the loaded microengine system. They were 1150 Hz and 1875, respectively. For all experiments, we accelerated the load gear to full speed in three rotations of the drive gear. This method was necessary to account for the inertia of the large gear.

The dice were packaged with glass covers to allow viewing of the rotating gears. The covers were taped on so they prevented particle contamination but allowed access to the ambient environment of the laboratory. The packages were stored in a dry nitrogen environment before the test. The tester, Sandia High Volume Measurement of Micromachine Reliability (SHiMMeR)[7], was used to provide electrical signals to large numbers of packaged microengines driving loads and to optically inspect them for functionality.

We performed stress tests at eight frequencies, 860, 1204, 1500, 1720, 2064, 2200, 2408, and 3000 Hz. The resonant frequency of the system was 1150 Hz which allowed for stresses both above and below resonance. The stress intervals followed roughly the same sequence for all the experiments. The sequence was 2000, 4000, 8000, 16000, …, rotation cycles of the drive gear per stress. If more than 4 parts failed during a particular stress, we repeated that stress interval. The devices were stressed at high speed and then slowed to 1 Hz to inspect for functionality. A failure was defined as the inability of the microengine drive gear to make a complete revolution at the 1 Hz inspection speed. During the inspection interval, we noted any observed changes or degradation in the motion of the gears for our records.

4. RESULTS AND DISCUSSION

4.1 Data Analysis

Because the parts were observed at fixed inspection times, common to all the parts, the results fall into the category of reliability data called "interval" data. We plotted the accumulated number of cycles to failure against the cumulative percent failure for each stress frequency. The lognormal fit resulted in an estimate of t_{50}, the median cycles to failure. The estimate for the lognormal shape parameter, σ, was also determined.

The experimental results for the microengines driving loads with the pin linkage are listed in Table 1. We performed ten experiments and failed a total of 277 parts.

Most of the data from each of the experiments could be described by a simple unimodal distribution such as seen in Figure 4. In this figure, the first point and last two points were omitted from the fit. The regression analysis yielded a median cycles to failure of 1.6 x 10^5 cycles with σ = .37. The last two points could be the onset of another stronger population since bimodal distributions were observed in two of the frequency experiments.

Table 2 shows the results of lognormal fits to all of the frequency experiments. The data is also graphically repre-

Table 1. Series of frequency experiments performed.

f (Hz)	f/f_o	# Parts on test	# Parts Failed	# stress intervals
860	0.75	33	33	30
1204	1.05	45	41	23
1500	1.30	10	10	21
1500	1.30	42	42	30
1720	1.50	23	23	30
2064	1.79	32	32	40
2200	1.91	26	26	17
2408	2.09	28	27	27
3000	2.61	13	13	23
3000	2.61	40	40	23

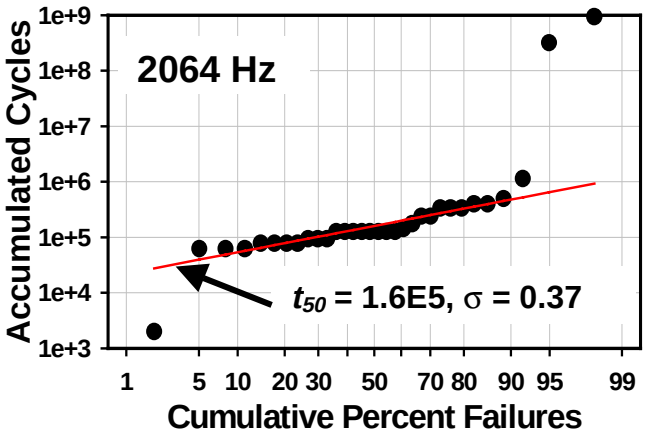

Figure 4. Lognormal distribution of accumulated cycles to failure for the 2064 Hz stress. The lower and upper freak data points were omitted from the regression analysis.

Table 2. Results of median number of cycles to failure from all frequency experiments performed.

f (Hz)	f/f_o	t_{50}	σ
860	0.75	8.50E4	0.35
1204	1.05	1.60E5	0.22
1500	1.30	1.29E5	0.65
1720	1.50	2.6E5	0.25
2064	1.79	1.60E5	0.37
2200	1.91	1.02E5	0.25
2408	2.09	7.20E4	0.26
3000	2.61	2.33E5	0.39

sented in Figure 5 with 90% confidence bounds represented by error bars.

For the stress frequencies of 1500 and 3000Hz, we repeated the experiments and the results of the second experiment were within the 90% confidence bounds of the first experiment. We then averaged the two results. This was an excellent demonstration of lot to lot repeatability since the microengines in the second experiment were from a different fabrication lot but of the same technology and design.

4.4.1 Experimental Observations

The behavior of the microengines as they were stressed followed a consistent pattern. Initially the microengines ran smoothly. With the accumulation of stress, the operation of the microengines became sticky and jerky (stick-slip behavior) at inspection frequencies. Some of the microengines would actually work through the sticky behavior and become smooth again. Near the end of life, the rotation became more erratic until the microengine failed by sticking or rocking back and forth through a small angle.

After failure, the part was still being stimulated by the drive signals so we optically panned across the entire microengine to get clues about the failure. We observed cases where the drive gear/load gear combination appeared stuck since we could see slight movement in the adjoining comb drives and shuttles. In other cases, the pin joint of the drive gear appeared to be stuck. Nearly half of the devices in this experiment failed with the Y shuttle stuck indicating that this was the dominant failure mode.

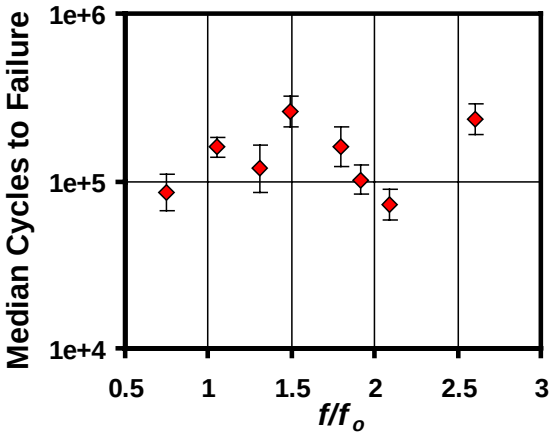

Figure 5. The frequency dependence of the lifetime of the microengines with pin linkages driving a load. The error bars represent 90% confidence bounds.

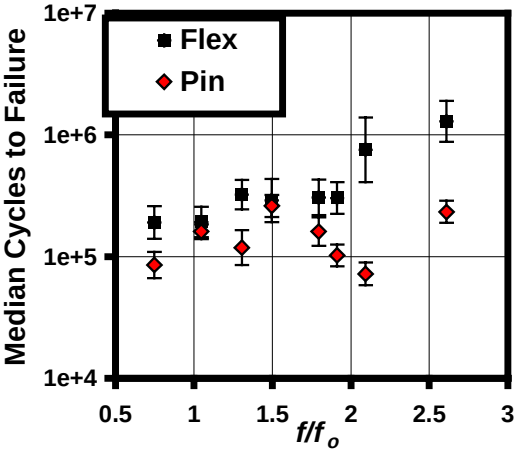

Figure 6. This comparison of median cycles to failure between the flexure linkage and the pin linkage shows the pin linkage to be less reliable.

4.1.2 Comparison of flex to pin

The flexure microengine reliability study was documented in reference 1. We compare the two by plotting the median number of cycles to failure against the ratio of the stress frequency to the resonant frequency. As seen in Figure 6, all of the experiments with pin linkages have lower median cycles to failure than the flex linkage thus implying lower reliability.

4.2 Failure Analysis

Failure analysis on the pin linkage microengine driving a load has proceeded in much the same way as its counterpart, the flex linkage system[1]. It was possible to optically document the existences of wear debris at drive gear hubs and, occasionally, its broadcast over the top of the gear from the drive pin region. It was also possible to document its absence from the load gear hub. These observations are from top view images into the gap between the hub and the gear.

Wear debris observations were corroborated in SEM imaging as shown in Figure 7. Arrows at right and in the center show wear debris in and on the hub of a drive gear that has been driven to 62,000 cycles. Lift-off techniques were used to remove drive gears for an inspection of the underside, as

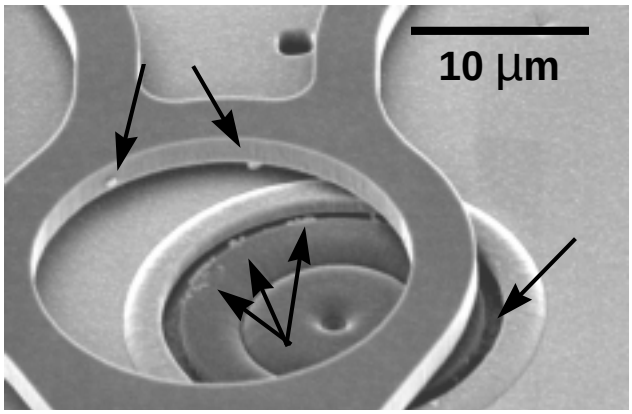

Figure 7. Wear debris in SEM image of drive gear and hub from pinned joint microengine tested to 62,000 cycles.

shown in Figure 8. The drive pin flange appears in the center of the image, with wear debris that has been broadcast over the horizontal surface between the flange and gear, and emerges at the perimeter of the pin flange. A similar effect occurs for the drive-gear hub lower flange, as seen in the lower right of the image.

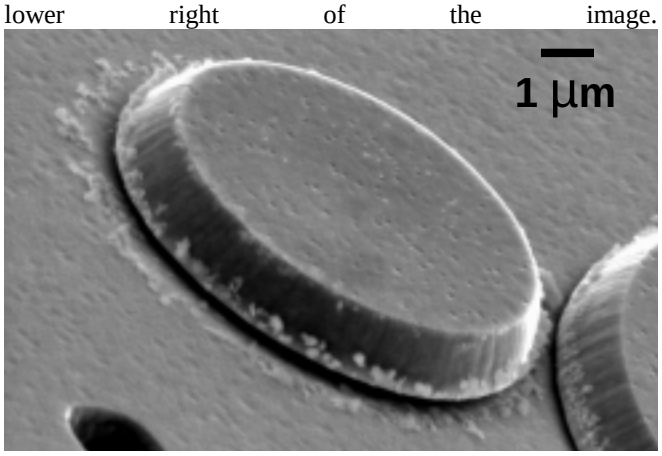

Figure 8. Wear debris as seen from the bottom of the gear, around the drive pin flange (center) and hub lower flange (lower right).

Load gear hubs were characteristically free from wear debris as in earlier work[1]. A comparison of worn and wear-free bearing interfaces is shown in Figure 9. These images are SEM photomicrographs of FIB sections performed on pin linkage microengines. The gaps between gear and flange surfaces characteristically fill with debris on drive gears, and are free from debris or any evidence of wear on load gears. All wear debris observations suffer from the fact that in the current test setup, all engines continue to receive drive signals until all engines on a die fail. In this way, a gear may be permitted to vibrate for a significant period after being considered a failure. Future testing will be conducted to alleviate this condition and provide more detailed snapshot at early wear debris observations. Such observations have been made at other locations on the engine, namely shuttles that reciprocate between guides.

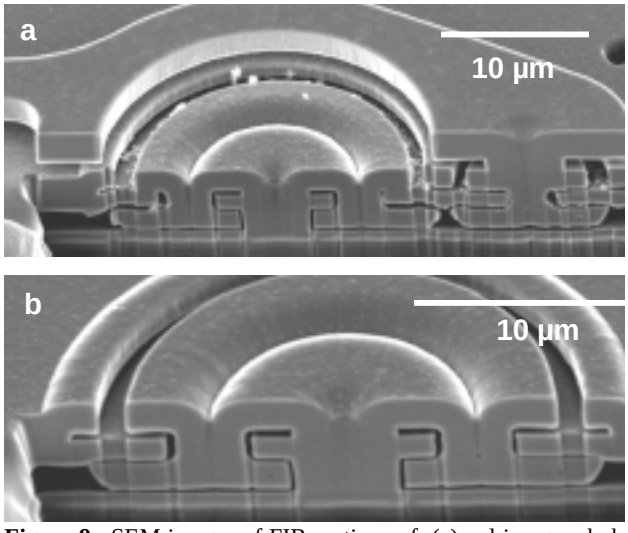

Figure 9. SEM images of FIB sections of (a) a drive gear hub and a drive pin and (b) a load gear hub from a pin linkage microengine operated to failure.

Pin linkage shuttles have a pin joint at the link between the Y shuttle (Fig. 3) and its link arm. This link is accompanied by structures anchored to the substrate, which serve to restrain the shuttle and link arm both laterally and vertically. The long guide at the shuttle includes a vertical oblong dimple extending downward. The horizontal surfaces at the link arm are planar. The surface between these guides and the actuating structures is an additional site where wear can occur on pin linkage engines. This wear is shown in Figure 10a to occur both at the half-round guide and the long shuttle guide. The wear track shown on the right in Figure 10a is further magnified in Figures 10b and 10c. The extent of the

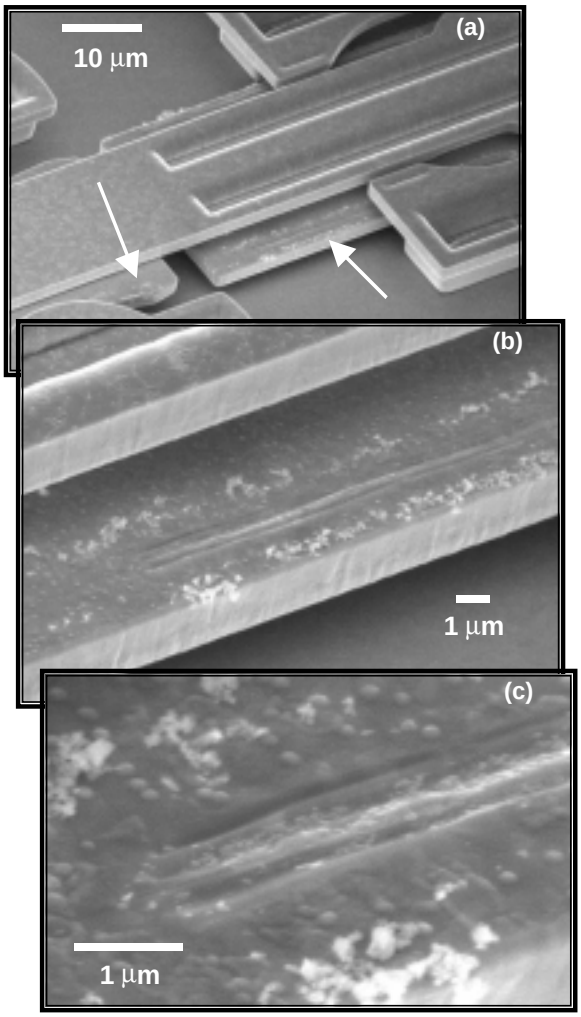

Figure 10. Wear debris and deep grooving of the shuttle from the dimples in the guides at successively higher magnification. These images were from a pin linkage microengine stressed at 1720 Hz for 290,000 cycles

reciprocation is such that the long shuttle guide with the dimples contacts only the shuttle and the half-round guides contact only the link arm.

We optically inspected 99 pin linkage microengines and found that 57% had wear tracks characteristic of abrasive wear. All had wear debris much like we observed in reference 1 which we attributed to adhesive wear. Tracks were observed on microengines with only 2000 cycles of stress. However, many microengines had over 10^6 (one near 10^9) with no wear tracks. The data were sorted according to the drive frequency, number of cycles to failure and whether a track was observed and **no** pattern was found. Wear track formation appears to be a random occurrence.

In several cases, optical examination of microengines being exercised with a drive cycle indicated that the Y shuttle was incapable of movement. Often, this is accompanied by other indicators such as cyclic flexing of the shuttle resulting in vertical displacement, or movement of the Y link arm up to the link pin under the action of the X shuttle. The X shuttle operates normally in all cases where it has been excised from the rest of the system.

Figure 11 shows a high tilt angle view of the pin linkage region of such an engine. Proximity or contact, although recorded where possible, is not a certain indicator of adherence between rubbing surfaces in our experience. At high tilt, the dimple (high magnification - upper right) appears not to be in contact with the shuttle although severe wear debris has been generated. The half round guide (lower right) appears to be in contact with the link arm.

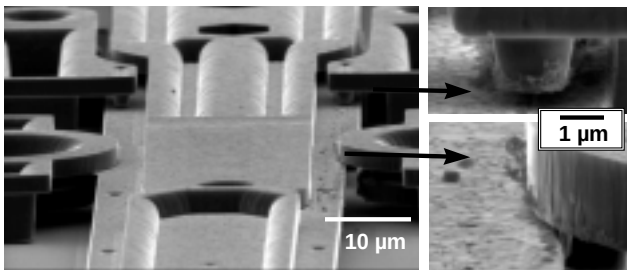

Figure 11. High-tilt SEM view of guide area and magnified views of guides.

Frequently, the shuttle was severely grooved on one side and less damaged on the other, indicating that the shuttle was canted during operation. The dimples appeared to have horizontal, smooth bottoms as indicated by control samples. FIB sections of one shuttle indicate asperities from rubbing which correspond to grooves in the shuttles.

In several instances, the FIB was successfully used to sever the connection between the portion of the guide supporting the dimple and the shuttle. A view of the placement of such a cut is shown in Figure 12.

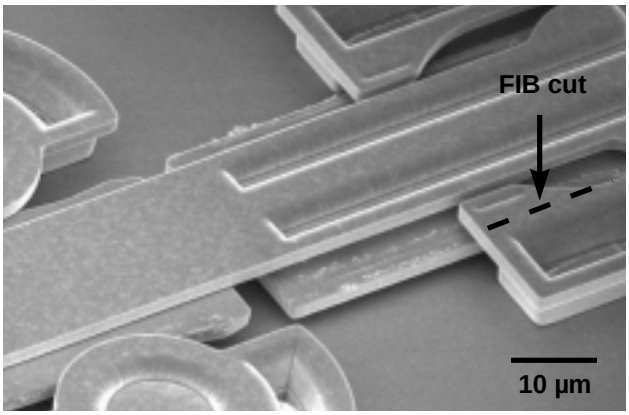

Figure 12. Location of FIB cut on pin linkage guide.

Two effects were observed. When the dimple was stuck to the shuttle, as the ion beam milled through the last remaining thickness of the guide, the springs of the comb drive restored the shuttle to its equilibrium position, carrying the remnant of the guide and stuck dimple as shown in Figure 13. Subsequent operation of these engines was restored by FIB cuts such as these.

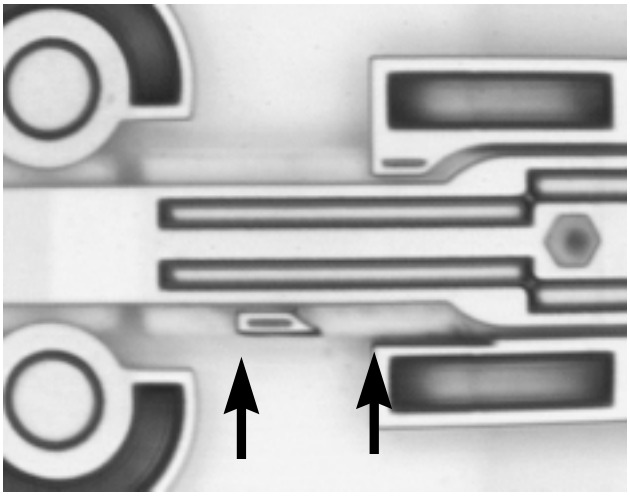

Figure 13. Optical image of a shuttle with an attached dimple that was freed from the anchored portion of the guide by a FIB cut. The shuttle moved to the left with no external force applied to the engine.

Linkage pins attached to the Y shuttles and receiver holes in the connecting arms also show some evidence of directional wear. This has been corroborated by FIB sectioning and is shown in the SEM images of Figures 14 and 15. Pin wear was predominantly on faces perpendicular to the direction of motion of the shuttle. The worn receiver hole in Figure 15 is viewed from the top surface, and the control sample is viewed from the bottom surface, which was exposed when it was lifted off. The wear resulting form operation is quite evident.

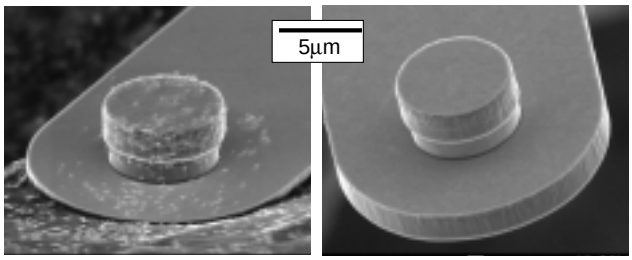

Figure 14. Linkage pins from a failed engine (left) and from a control sample (right).

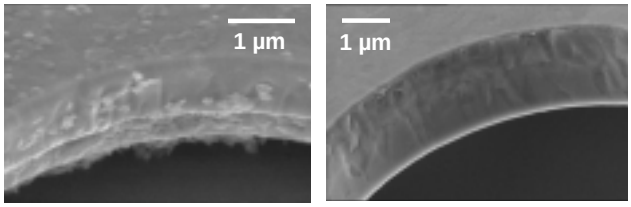

Figure 15. Receiver holes in link arms. Top view on engine worn to failure (left) and view of bottom surface of engine which was never operated (right).

Figure 16 is an SEM image at 0^o tilt angle that shows a typical result for pin joint receiver holes in drive gears in both flex linkage and pin linkage microengines tested to failure. The wear debris is generated somewhat more severely at drive pins than at drive hubs. Many receiver holes show this appearance of material having been "scooped out" from the bore on one side and wear debris piled up in another site—effectively changing the location of the hole. Compare this to the round appearance of the hub attachment pillar and lower hub flange on the right of the image. This engine failed into a rocking mode; it did not seize up completely. A magnified view of this hole is shown in Figure 17.

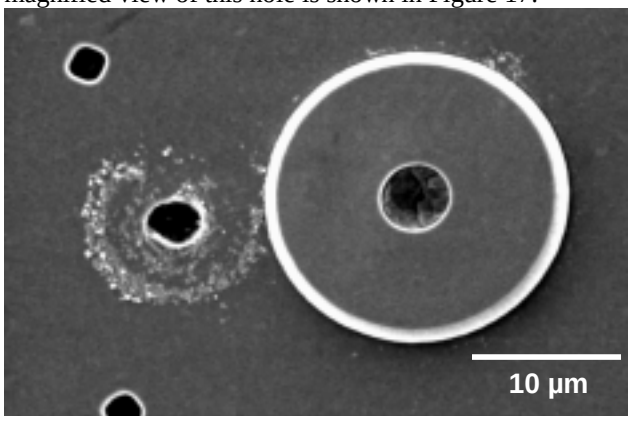

Figure 16. SEM image of receiver hole in drive gear exhibiting severe wear.

4.2.1 FA Summary

Both pin linkage and flex linkage microengines driving load gears experienced significant wear which was most severe at pins and receivers in the drive gear, and also frequently found on drive gear hubs. No instance of wear debris has been observed on load gear hubs of pin linkage microengines driving loads. Significant wear has been found at locations unique to the pin linkage microengines, such as pins and holes and restraining guides and shuttles. The occurrence of debris on the Y shuttle guides of the flex linkage engines has been somewhat lower. The guides on the flex linkage engine have 0.5-micron spacing and are not clamped with a dimple from the upper layer of polysilicon.

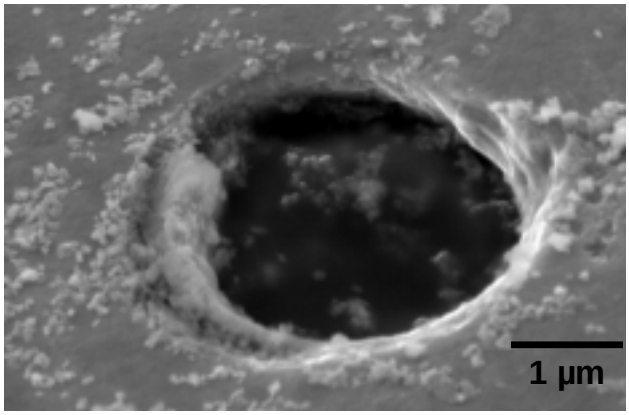

Figure 17. Drive gear receiver hole in a pin linkage microengine tested to failure.

Additional studies are planned of the wear debris, to view different stages in its generation and to understand its morphology and properties in greater detail.

4.3 Model Development – Adhesive and Abrasive Wear

It is critical that a failure model be developed that describes the observed physics of failure and allows prediction of ultimate failure in any final design. To do so the failure modes must be established from statistically significant data.

4.3.1 Failure Modes

There are seven primary wear failure mechanisms observed for macroscopic mechanical systems[11]: adhesion, abrasion, corrosion, surface fatigue, deformation, impact, and fretting wear. Due to the microscopic nature of each of these mechanisms, we would expect that one or a combination of them (as opposed to some other mechanism) would be responsible for the wear-out of the micromachines described in this paper.

It has been previously observed in these microengines that the friction forces change abruptly[9]. At relatively low normal forces sticking and wear particle formation has been observed that we attribute to adhesive wear[1]. For higher normal forces we would expect to observe wear tracks[12] characteristic of abrasive wear[11]. That we did observe wear tracks, in 57% of the parts examined indicates that abrasive wear was taking place, possibly in conjunction with adhesive wear.

There was no evidence of corrosion by-products, ruling this wear mechanism out. Finally, surface fatigue, deformation and impact wear typically require forces well in excess

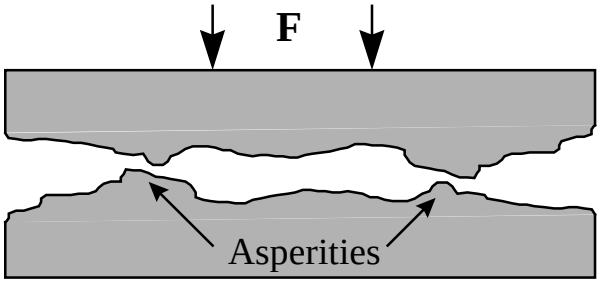

Figure 18a. Force F brings the two surfaces into contact at the asperities.

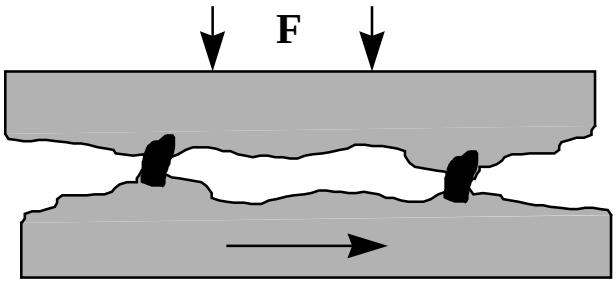

Figure 18b. As the lower surface moves, the asperities cold weld together.

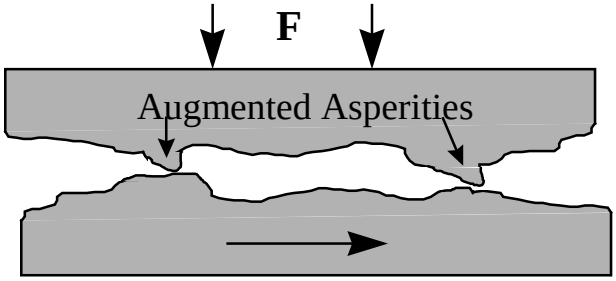

Figure 18c. As the lower surface continues to move, the material breaks free again, leading to the augmented asperities on the upper surface or loose particles.

of those for abrasive wear. Again such forces were not applied. Fretting wear occurs when machine elements experience fluctuating loads, leading to microcracks and ultimately failure by fatigue. Microcracks have also not been observed.

Therefore, our emphasis will be on describing the observed failures in terms of lower pressure adhesive wear and higher pressure abrasive wear.

4.3.2 Adhesive Failure Model: Lower Pressure Effects

At pressures low enough not to result in gouging of the surface and the production of wear tracks, adhesive wear can occur. This has been observed in pin joints of these microengines in the past[1]. Adhesive wear occurs when contact of asperities between two solid bodies (Figure 18a) leads to plastic flow and cold welding (Figure 18b). The asperity then tears away, leaving a particle transferred to one surface (Figure 18c). In this way, material can transfer from one surface to another and result in regions where the micromachine can begin to catch and then fail, as observed.

The derivation of the model for adhesive failure begins by assuming that there is some critical volume, V_c, of material that must be transferred in order to stop the motion of the micromachine. We anticipate that V_c is not a single number but is a distribution of values. We will make a point estimate of this value later.

In adhesive wear, the relationship between the wear volume ΔV, and the length of the motion producing the wear, ΔL is given as[11]:

$$\Delta V = \Delta L\left(\frac{KF}{9\sigma_{yp}}\right) \tag{1}$$

where K is the adhesive wear constant
F is the force on the joint and
σ_{yp} is the uniaxial yield strength

The total length of the motion at the guide where the wear was observed (Fig. 10) is just four times the distance from the drive gear hub center to the location of the pin joint, r', on the drive gear and the number of revolutions, R, that the microengine makes.

$$\Delta L = 4r'R \tag{2}$$

Combining equations (1) and (2), and setting ΔV to V_c, the critical volume for failure, F the force applied normal to the guide to be F_N and R to $R_{f(adh)}$, the number of revolutions to failure for adhesive wear and solving for $R_{f(adh)}$ we get:

$$R_{f(adh)} = \left(\frac{9}{4}\right)\left(\frac{\sigma_{yp}}{K}\right)\frac{V_c}{r'F_N} \tag{3}$$

4.3.3 Abrasive Failure Model: Higher Pressure Effects

Abrasive wear (example shown in Figure 19) may take place where a hard asperity on one surface gouges or wears another mating surface. This is commonly called two-body wear. Likewise a hard particle trapped between two surfaces can lead to gouging and wear in what is called three-body wear[11]. We will assume that work-hardened asperities or particles may result in the gouging seen in the surface of the wearing surface and will further assume that the shape of this asperity is roughly conical and that only a single asperity actually makes contact and creates the wear. The penetration of this asperity will be such that the normal force, F_N applied

to it divided by the contact area, A is equal to the flow stress in the polysilicon[11]. Thus,

$$F_N = 3A\sigma_{yp} \tag{4}$$

Given that the asperity is assumed to be conical, the contact area, A, can be written as:

$$A = \frac{\pi}{4}W^2 \tag{5}$$

And hence the forces balance when:

$$F_N = \frac{3\pi}{4}W^2\sigma_{yp} \tag{6}$$

where the width of the groove is given as W.

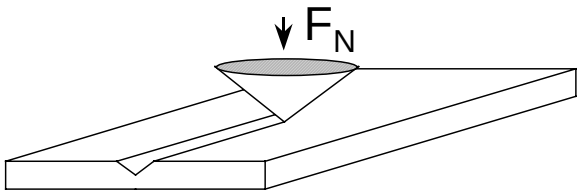

Figure 19a. Example of how abrasive wear occurs. An

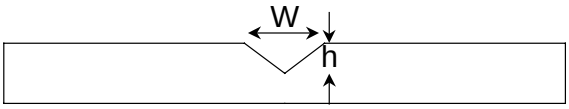

Figure 19b. Definitions of groove parameters used in abrasive wear derivations.

The abrasive wear volume, V_{abr} swept out by the per cycle is then given as:

$$V_{abr} = Wh\Delta L\alpha \tag{7}$$

where the height of the groove is given as *h* and the total wear length is given as ΔL. The constant α is the reciprocal of the total number of cycles to produce the wear track of height, *h*, and width, *W*. Replacing the wear length with its value given in equation (2) yields:

$$V_{abr} = 4r'RWh\alpha \tag{8}$$

By substituting the value for W obtained by inverting equation (6) into the expression for the abrasive wear volume in equation (8) we may write:

$$V_{abr} = \sqrt{\frac{64F_N}{3\pi\sigma_{yp}}}hr'R\alpha \tag{9}$$

Just as for adhesive wear, when the wear volume equals some critical volume (described below) we would expect the device to fail. Thus, we can use equation (9) setting V_{abr} to V_c and R to $R_{f(abr)}$ (the number of revolutions to failure for abrasive wear) to get:

$$R_{f(abr)} = \frac{V_c}{\alpha hr'}\sqrt{\frac{3\pi\sigma_{yp}}{64F_N}} \tag{10}$$

4.3.4 Resonance Effects:

The true normal force on the guide will vary with excitation frequency, ω, as the critical frequency, ω_o, for resonance is approached due to variations in forces caused by the inertia of the system and the tolerance in the pin joints. The joints have approximately 50% tolerance as measured by the total diametrical gap divided by the joint size.

In such a case, the normal force, F_N on the guide will increase as the frequency approaches the critical frequency as[13]:

$$F_N = F_n\left[\frac{1}{\sqrt{\left[1-\left(\frac{\omega}{\omega_o}\right)^2\right]^2+\left(\frac{1}{Q}\frac{\omega}{\omega_o}\right)^2}}\right] \tag{11}$$

where the term in large square brackets represents a "magnification factor" caused by approach to resonance and

F_n is the nominal force applied to the guide,

Q is the "quality factor" of the damped harmonic mechanical system and

ω / ω_o is the ratio of the driving frequency to the resonant frequency of the system.

4.3.5 Combined Adhesive/Abrasive Wear Model:

Combining equations (3), (10) and (11) we now arrive at the description for the reliability of a MEMS actuator failing due to adhesive and abrasive wear occurring between the guide and the Y-shuttle of the microengine. The mechanism that leads to the earliest failure will predominate.

$$R_{f(adh)} = \left(\frac{9}{2\pi}\right)\left(\frac{\sigma_{yp}}{K}\right)\frac{V_c}{r' F_n}\times \left[\sqrt{\left[1-\left(\frac{\omega}{\omega_o}\right)^2\right]^2+\left(\frac{1}{Q}\frac{\omega}{\omega_o}\right)^2}\right] \quad (12)$$

$$R_{f(abr)} = \frac{V_c}{8\alpha h r'}\times \sqrt{\frac{3\pi\sigma_{yp}}{F_n}\sqrt{\left[1-\left(\frac{\omega}{\omega_0}\right)^2\right]^2+\left(\frac{1}{Q}\frac{\omega}{\omega_0}\right)^2}} \quad (13)$$

In addition, we include the formula for the number of revolutions to failure when the wear occurs mainly in the pin joint of the drive gear. This was derived in reference 1. The variables are identical to equations (12) and (13). The variable, *r*, was the radius of the pin joint located in the drive gear.

$$R_f = \left(\frac{9}{2\pi}\right)\left(\frac{\sigma_{yp}}{K}\right)\frac{V_c}{rF_n}\times \left[\sqrt{\left[1-\left(\frac{\omega}{\omega_o}\right)^2\right]^2+\left(\frac{1}{Q}\frac{\omega}{\omega_o}\right)^2}\right] \quad (14)$$

Note that there are no adjustable fit parameters. The physical constant variables that are material dependent are known or can be estimated. The other variables have been measured or calculated.

V_c, the critical volume of adhered material, can be estimated from known physical parameters[14] by calculating the size of an asperity needed to stop the motion of the guide after a cold weld occurs (Figure 18b). The cross-sectional area of such a weld that can just stop the motion of the shuttle is given as:

$$A_c = F_\ell / \sigma_{yp} \quad (15)$$

where A_c is the "critical area" of the cold weld and F_ℓ is the longitudinal force exerted by the moving shuttle. F_ℓ was measured by displacing a cantilever beam with known physical parameters with the shuttle. The maximum drive voltage of 80V was used to produce a force of 11.8 μN.

If one assumes a roughly cubic mass of material with this critical area, then the critical volume of this mass is given by:

$$V_c = A_c^{3/2} = \left[F_\ell / \sigma_{yp}\right]^{3/2} \quad (16)$$

For the values of force and yield strength given in table 1, we calculate a value of 9.75 x 10^{-4} μm^3 for V_c.

The normal force was calculated using a model of a single layer comb. The maximum levitation force at a voltage of 80 V was determined to be 39 μN. Since this is the value at one extreme, we used an average value of 19.5 μN.

The adhesive wear constant for polysilicon on polysilicon hasn't been measured. The value in Table 1 was an estimate from experiments of ceramic on ceramic.

4.3.6 Comparison to Model

Table 1 has the values of the model parameters and the corresponding references. Figure 20 shows the measured reliability data as compared to the various models. The data are bounded between the two adhesive models. The pin-joint adhesive wear model assumes the dominant wear occurs in the pin joint of the drive gear. In the linkage adhesive wear model, the assumption is that the dominant wear occurs in the Y-shuttle linkage. The linkage abrasive wear model describes wear occurring in the Y-shuttle linkage.

Table 1. Failure Model Parameters

Variable	Parameter	Value	Ref.
σ_{yp}	uniaxial yield strength	1.2x10^{-3} N/μm^2	[14]
K	adhesive wear constant	4x10^{-7}	[15]
V_c	critical volume	9.75x10^{-4} μm^3	calculated
r'	Hub to pin joint radius	17 μm	design
F_n	Normal force	19.5 μN	calculated
ω_o	Resonant freq.	1150 Hz	measured
Q	Quality factor	1.1	measured
F_ℓ	Longitudinal force	11.8 μN	measured
α	Cycle constant	3.5 x 10^{-6}	measured
H	Height of track	67 nm	measured

It is surprising that the abrasive model did so poorly. We definitely have instances of abrasive wear since we observed wear tracks. However, we also observed large amounts of wear particles associated with adhesive wear. It is possible that a particle lodged between the dimple and the shuttle formed the track and then broke off leading to more adhesive wear.

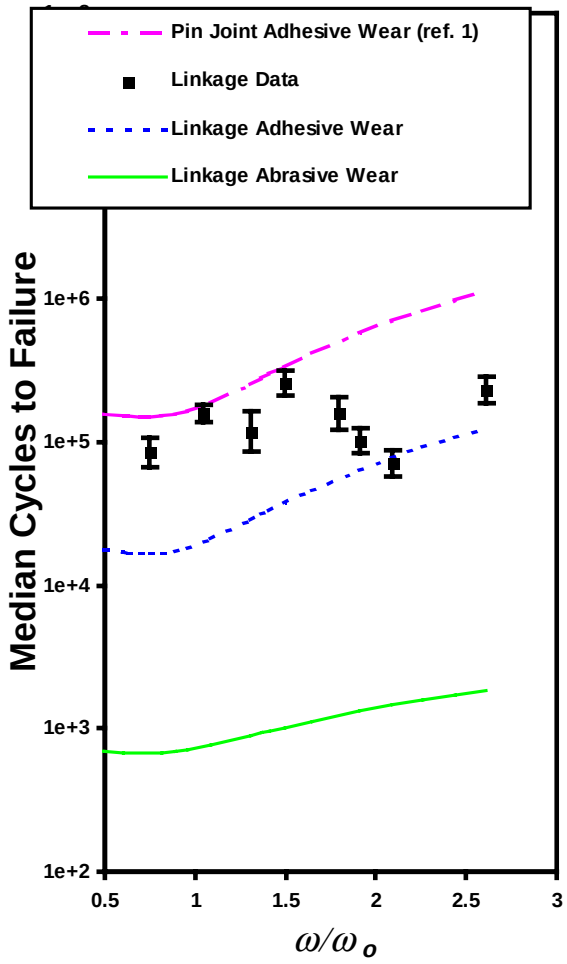

Figure 20. Pin linkage data compared to the various wear models.

5. CONCLUSIONS

We have determined that the pin mechanism linkage is less reliable than the flexure linkage. This was due to the tight tolerance (0.5 μm) of the guides that prevent vertical motion. We observed excessive wear debris and wear tracks due to the rubbing of the dimple and the moving shuttle. The wear tracks appear on microengines with low accumulated cycles and high accumulated cycles. Many microengines failed with no observable wear tracks.

We have presented an adhesive wear model which bounds the data indicating that the failures were a combination of wear occurring in the drive gear pin joint and wear occurring between the dimple and the Y shuttle. However, abrasive wear was a factor since we observed wear tracks indicating that the abrasive model presented requires further study.

ACKNOWLEDGMENTS

Special thanks to Alex Pimentel for the FIB work and Karen Helgensen for performing the reliability tests on SHiMMeR. We are grateful to Larry Warne for performing calculations of the levitation force of the comb actuators. Donna Senft measured the longitudinal force of the comb actuators. We also thank the personnel of the Microelectronics Development Laboratory at SNL for fabricating, releasing, and packaging the devices used in the test.

Sandia is a multi-program laboratory operated by Sandia Corporation, a Lockheed Martin Company, for the United States Department of Energy under Contract DE-AC04-94AL85000.

REFERENCES

[1]D. M. Tanner, W. M. Miller, W. P. Eaton, L. W. Irwin, K. A. Peterson, M. T. Dugger, D. C. Senft, N. F. Smith, P. Tangyunyong and S. L. Miller, "The Effect of Frequency on the Lifetime of a Surface Micromachined Microengine Driving a Load," *1998 IEEE International Reliability Physics Proceedings, IRPS 98*, pp. 26-35 (1998).

[2]L. Spangler and C. J. Kemp, "ISAAC: integrated silicon automotive accelerometer," *Sensors and Actuators A*, **Vol. 54**, pp.523-529, 1996.

[3] S. Bart, J. Chang, T. Core, L. Foster, A. Olney, S. Sherman, W. Tsang, "Design Rules for a Reliable Surface Micromachined IC Sensor", *1995 IEEE International Reliability Physics Proceedings, IRPS 95*, pp. 311-317 (1995).

[4] T. Maudie, D. J. Monk, D. Zehrbach, and D. Stanerson, "Sensor Media Compatibility: Issues and Answers," *Proc. Of Sensors Expo*, Anaheim, CA, pp.215-229, April, 1996.

[5] W. P. Taylor and M. G. Allen, "A Packaging Compatible Fully Integrated Micromachine Relay," International Symposium on Microelectronics ,*Proc. SPIE*, **Vol. 2920**, pp. 202-207, 1996

[6] M. R. Douglass, "Lifetime Estimates and Unique Failure Mechanisms of the Digital Micromirror Device (DMD), *1998 IEEE International Reliability Physics Proceedings, IRPS 98*, pp. 9-16 (1998).

[7] D. M. Tanner, N. F. Smith, D. J. Bowman, W. P. Eaton, K. A. Peterson, " First Reliability Test of a Surface Micromachined Microengine Using SHiMMeR," *Proceedings SPIE Symposium on Micromachining and Microfabrication*, **Vol. 3224**, Austin, 1997, pp 14-23.

[8] E. J. Garcia and J. J. Sniegowski, "Surface micromachined microengine", Sensors and Actuators A, **Vol. 48**, 1995, pp. 203-214.

[9] S. L. Miller, J. J. Sniegowski, G. LaVigne, and P. J. McWhorter, "Friction in Surface Micromachined Microengines", *Proceedings of SPIE Smart Electronics and*

MEMS **Vol. 2722**, San Diego, Feb. 28-29, 1996, pp. 197-204.

[10]S. L. Miller, J. J. Sniegowski, G. LaVigne, and P. J. McWhorter, "Performance tradeoffs for a surface micromachined microengine", *Proceedings of SPIE Micromachined Devices and Components II*, **Vol. 2882**, Austin, October. 14-15, 1996, pp. 182-191.

[11]J. A. Collins, *Failure of Materials in Mechanical Design*, New York, John Wiley & Sons, Inc., 1981.

[12]D. C. Senft and M. T. Dugger, " Friction and wear in surface micromachined tribological test devices," *Proceedings SPIE Symposium on Micromachining and Microfabrication*, **Vol. 3224**, Austin, 1997, pp 31-38.

[13]C. R. Freberg and E. N. Kemler , *Elements of Mechanical Vibration, 2nd ed.*, New York, John Wiley & Sons, Inc. (1949).

[14]W. N. Sharpe, Jr., B. Yuan, R. Vaidyanathan and R. L. Edwards, "Measurements of Young's Modulus, Poisson's Ratio and Tensile Strength of Polysilicon," *Proc. MEMS 97, 10th IEEE Inter. Workshop on MicroElectroMechanical Systems*, pp. 424-429.

[15]Ernest Rabinowicz, *Friction and Wear of Materials*, 2nd ed., New York, John Wiley & Sons, Inc., 1995.